ARTICLE OPEN

Check for updates

Compatibility of ethylene vinyl acetate (EVA)/ethylene vinyl alcohol (EVOH)/EVA films with gamma, electron-beam, and X-ray irradiation

Yelin Ni[1]✉, Tucker T. Bisel[1,8], Md Kamrul Hasan[2,9], Donghui Li[1], Witold K. Fuchs[1,10], Scott K. Cooley[1], Larry Nichols[3], Matt Pharr[2], Nathalie Dupuy[4], Sylvain R. A. Marque[5], Mark K. Murphy[1], Suresh D. Pillai[6], Samuel Dorey[7]✉ and Leonard S. Fifield[1]✉

Many polymer-based medical devices are sterilized by gamma irradiation. To reduce the use of cobalt-60 gamma-ray sources, transition from gamma ray to alternative irradiation technologies was proposed, namely electron beam (e-beam) and X-ray. A major impediment for such a transition is the knowledge gap in material compatibility with the different radiation sources. In this study, multi-layer films consisting of ethylene vinyl acetate (EVA) and ethylene vinyl alcohol (EVOH) components were irradiated to target doses of 30, 45, and 60 kGy by gamma-ray, e-beam, and X-ray sources. Effects of irradiation were evaluated on 12 material properties, and statistical comparisons between gamma irradiation and alternative technologies were conducted using the two one-sided t-test (or "equivalence test") and classic t-test. Melting temperature and UV absorbance below 300 nm showed dose dependencies, while other investigated properties such as discoloration and mechanical durability did not change with dose up to 60 kGy. Based on these results, there is no material compatibility issue associated with the transition from gamma to e-beam or to X-ray as source of sterilization radiation of the studied multi-layer film.

npj Materials Degradation (2023)7:93 ; https://doi.org/10.1038/s41529-023-00413-x

INTRODUCTION

Single-use, sterile plastic bags have been used in food and biopharmaceutical packages with the advantages of low cost and minimized potential cross-contamination. These packaging materials are required to be flexible, airtight, watertight, and optically clear. Multi-layer or polymer blend films have been designed to meet these requirements.

Sterilization is a critical step to prepare these packages for microbiological safety. Currently, for the medical devices and healthcare products that use ionizing radiation for sterilization, 40.5% of products are irradiated with cobalt-60 gamma rays, 4.5% with electron beams (e-beams), and less than <1% with X-rays[1,2]. The rising costs of cobalt-60, along with concerns of safety, security, and availability, are forcing the transition from cobalt-60 gamma irradiation to other alternatives, namely e-beam and X-ray irradiation. Regulatory acceptance of these alternative radiation sources requires testing of the compatibilities of the polymer products with the alternatives and comparing them to the compatibilities with the standard cobalt-60[2,3]. Ideally, the ionizing radiation source should have high microbicidal efficacy but cause minimal degradation. Studies on radiation microbicidal effectiveness[4,5] and modifications on material properties[6,7] have been reported for limited types of healthcare products, but a dataset of material compatibilities of common materials is still lacking.

The ionizing radiation can initiate photodegradation of polymers once a chemical bond absorbs the photon energy from radiation sources and free radicals form from the electronically excited states[8]. The free radicals propagate and result in various chemical reactions depending on the molecular structure and the ambient conditions[9]. Scission of polymer chains and crosslinking are the two main reactions, typically leading to deterioration of mechanical properties[10]. In ambient atmosphere, oxidation of carbon bonds follows the initiation and generate carbonyl species, which can be detected on Fourier Transform Infrared Spectrometry (FTIR). In commercial products, antioxidants and stabilizers are added to polymeric materials. The polymer itself and the additives can degrade to cause discoloration, often in the form of yellowing for initially white or transparent materials[11].

In this study, a multi-layer film plastic bag comprising of ethylene vinyl acetate (EVA) and ethylene vinyl alcohol (EVOH) copolymers was selected for testing. EVA is a barrier to water and EVOH is a barrier to oxygen and to carbon dioxide[12]. The two polymers also possess excellent durability, low-temperature toughness, and high optical transmission, and thus are good candidates for medical encapsulants[12,13]. EVA is also used in the encapsulation of photovoltaic modules, whose degradation behavior under UV radiation is a concern[14]. Discoloration from light yellow to dark brown was reported for EVA encapsulants after exposure to heat, UV and moisture[14], accompanied with the broadening of the peak in carbonyl region (near 1740 cm^{-1}) on FTIR[15]. Tensile strength and elongation at break of EVA were reported to decrease dramatically after 800 h of thermal-UV aging, due to chain scission as evident by a remarkable drop in molecular weight[16]. Melting temperature of EVA increased by 2 °C after 127 kWh m^{-2} UV exposure at 60 °C, and by 20 °C after 200 kWh m^{-2}, the latter of which was attributed to deacetylation which could be considered as chemical degradation[17]. The surface of an EVA-based adhesive was modified by 5-min UV treatment where surface energy and wettability increased

[1]Pacific Northwest National Laboratory, Richland, WA 99354, USA. [2]Department of Mechanical Engineering, Texas A&M University, College Station, TX 77843, USA. [3]Steri-Tek, Fremont, CA 94538, USA. [4]Aix Marseille Université, Avignon Université, CNRS, IRD, IMBE, 13013 Marseille, France. [5]Aix Marseille Université, Case 551, CNRS, ICR, 13397 Marseille, France. [6]National Center for Electron Beam Research, Texas A&M University, College Station, TX 77845, USA. [7]Sartorius Stedim FMT S.A.S., 13400 Aubagne, France. [8]Present address: Washington River Protection Solutions, Richland, WA 99352, USA. [9]Present address: Pacific Northwest National Laboratory, Richland, WA 99354, USA. [10]Present address: NASA Glenn Research Center, Cleveland, OH 44135, USA. ✉email: yelin.ni@pnnl.gov; samuel.dorey@sartorius.com; leo.fifield@pnnl.gov

Table 1. Statistical testing results to examine equivalence between gamma irradiation vs. alternative technologies (e-beam and X-ray) in terms of their effects on polymer material properties.

Material Properties	Metrics/Datasets	Industrial equivalency criteria for TOST	TOST conclusion based on industrial equivalency criteria	*T*-test conclusion (95% confidence level)
Coloration	Yellowness index, YI	N/A	-	ND
	Total color difference, ΔE	<2	E	ND
Thermal	Melting temperature, T_m	<5 °C	E	CC
	Degree of crystallinity, χ_c	N/A	-	ND
	Glass transition temperature, T_g	<5 °C	E	ND
Mechanical	Elongation at break, EAB	<25% loss	E	ND
	Ultimate tensile strength, UTS	<35% change	E	ND
	Secant modulus, Es	N/A	-	ND
	Tensile toughness, U_T	N/A	-	ND
Spectro-scopic	UV (280 nm) absorption, Abs	N/A	-	CC
	Carbonyl index, CI	N/A	-	ND
	Surface free energy, SFE	N/A	-	ND

The conclusions of two one-sided *t*-test (TOST) were based on industrial criteria, and the conclusions of *t*-test were based on 95% confidence level. "E": can claim equivalence at all doses (30 kGy, 45 kGy, 60 kGy). "ND": not different at any of the three dose levels. "CC": cannot conclude on the equivalence with the current dataset. "N/A": not available.

with an increase in oxygen content[18]. The EVA/EVOH/EVA layered product irradiated using cobalt-60 gamma ray, e-beam, and X-ray sources was thoroughly tested (i) to identify photodegradation during sterilization in terms of discoloration, changes in thermal and mechanical properties, UV and FTIR spectra, and surface wettability; (ii) to explore the mechanism for any change in aforementioned properties if it shows a dose dependence; (iii) to evaluate material compatibilities of the three sterilization technologies based on statistical analyses of the material properties. Here we assume that the microbicidal effectiveness of different radiation sources is the same at the same radiation dose[4,5], and that a radiation technology would be more compatible if it causes less material degradation and smaller modification on material properties.

It was hypothesized that there would be equivalence in the material properties after exposure to equal doses of the alternative radiation sources as compared to cobalt-60 gamma radiation. Statistical tests were performed to evaluate the hypothesis. When the objective of a statistical hypothesis test is to conclude that data series are equivalent, an equivalence test should be utilized[19], and such use is described herein.

RESULTS

Spectroscopic, thermal, and mechanical properties of EVA/EVOH/EVA specimens after gamma ray, e-beam, and X-ray irradiation were measured and quantified as single-value indices, such as yellowness index, melting temperature, tensile elongation at break, etc. Using these single-value properties, comprehensive datasets were constructed for statistical comparison between the effects of radiation source, i.e., whether gamma and alternative technologies (e-beam and X-ray) cause the same degree of change in these material properties at the same doses. The answer to this question depends on the choice of comparison method (such as statistical testing method) and criteria (such as equivalency criteria or significance level). Since classical difference tests do not allow concluding parity in the case that the statistical test does not indicate a significant difference, equivalence tests were employed on our data to demonstrate sameness or similarity rather than showing differences between options. A common procedure used to perform equivalence analysis is the two one-sided *t*-test (TOST), which assumes that two sets of data are not equivalent until sufficient evidence is accumulated to prove equivalency. When using equivalence tests, the first step is to specify how large of a difference between the sets of data would represent a practically important difference. Smaller differences than the threshold are considered insignificant when comparing the sets of data and equivalence can then be concluded.

A set of industrial equivalency criteria provided by the film manufacturer was proposed for the TOST analysis, as listed in Table 1, to fill the current lack of standardized criteria of quantified equivalence limits in terms of polymer properties. Following industrial equivalence criteria, equivalence can be claimed for effects of gamma ray versus alternative technologies (e-beam and X-ray) on total color difference (ΔE), melting temperature (T_m), glass transition temperature (T_g), Tensile elongation at break and ultimate tensile strength.

An obvious limitation of the practice of using TOST and industrial equivalency criteria is that the criteria are summarized from test data accumulated during years-long research, and are not always available for all the material properties or metrics of interest. As a temporary mitigation, *t*-test with 95% confidence level was conducted and the results were given in Table 1. Based on *t*-test results, the majority of material properties are not different after gamma vs. e-beam or X-ray irradiation at same dose, except for two material properties where we cannot conclude on their equivalences, namely UV absorbance (Abs) near 280 nm wavelength and T_m.

There is an apparent contradiction on whether the effects of different radiation technologies on T_m. Based on TOST with industrial criteria, they were considered equivalent, but *t*-test result cannot conclude on the equivalence based on 95% confidence level. The reason for the different conclusions is because the 95% confidence level is a much stricter criterion due to a limited sample size and lack of randomization in *t*-test samples. Specifically, the sample size is only 3–6 replicates at each condition and the material property data used for statistical analyses were measured on films manufactured and irradiated in the same batch and using the same instrument. It should be noted that although *t*-tests were able to identify subtle differences

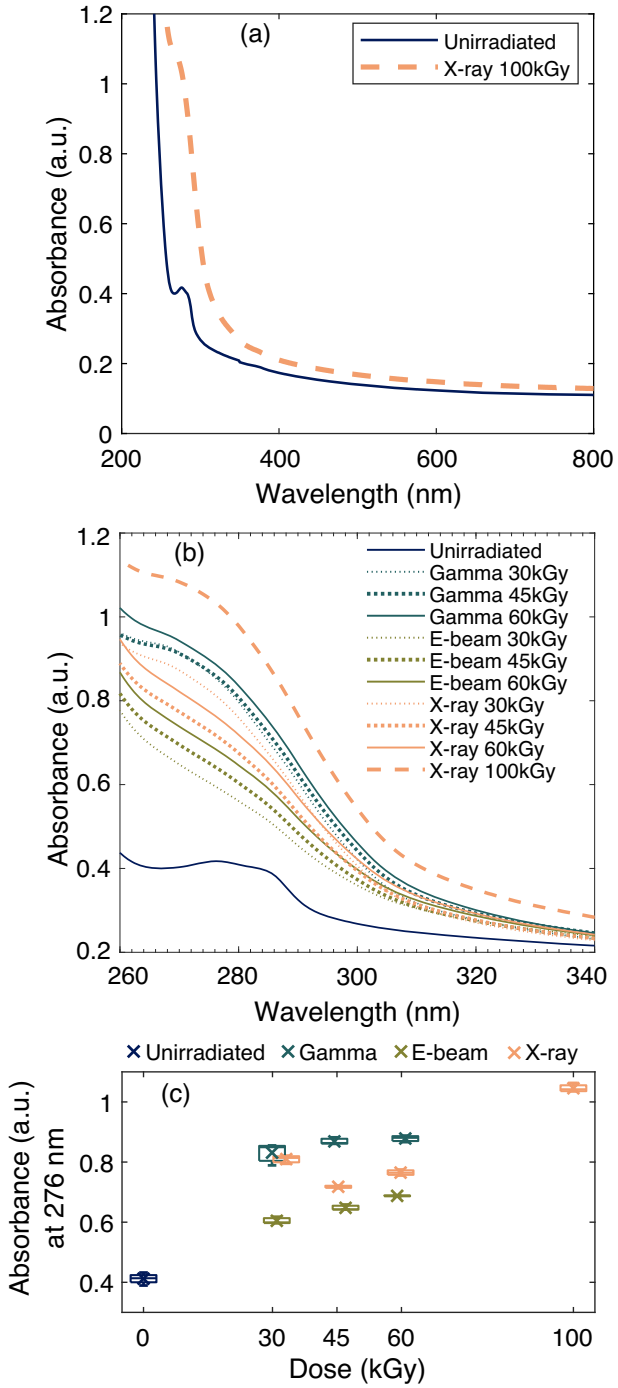

Fig. 1 UV absorbance of EVA/EVOH/EVA films. a UV absorbance of an unirradiated film compared to the maximum irradiation, i.e., 100 kGy under X-ray, in the full wavelength range. **b** UV absorbance in 260–340 nm wavelength of films irradiated at different doses and technologies. **c** UV absorbance at 276 nm as a function of actual delivered doses. On each box, the cross indicates the sample mean, the central line is the median, the bottom and top bounds of the box represent the 25th and 75th percentiles, and the whiskers extend to the extreme values which are within 1.5 times the interquartile range away from the box bounds.

between datasets, the ability to draw general conclusion regarding material compatibilities of sterilization technologies from the *t*-test results in Table 1 is limited. The *t*-test results can rather be used as a screening check to identify the material properties that might be more susceptible to a switch in radiation technology than other material properties. In this study, UV absorbance near 280 nm and T_m data will be further discussed in following sections in order to better understand what specific consequences may result if gamma radiation would be supplemented by e-beam or X-ray technology.

UV absorbance

UV absorbance (Abs) values between 200 nm and 800 nm are plotted in Fig. 1a for the unirradiated film and for the film exposed to a maximum dose of 100 kGy under X-ray irradiation. In the optical wavelength range (380–780 nm), the two curves are flat and almost overlap, where the Abs values in both curves are lower than 0.23 and their differences are smaller than 0.04 (relative difference smaller than 18%). This is consistent with UV absorbance behavior for generic EVA materials, which are transparent at wavelengths above 350 nm[14,20].

Abs values in a more focused wavelength range (260–340 nm) are displayed in Fig. 1b for all doses and irradiation technologies where one representative curve out of three replicates is plotted. The absorbance curve of unirradiated samples exhibits a wedged peak at 276 nm and a shoulder at 283 nm. The peak and shoulder shift to a shorter wavelength and become less pronounced as the dose increases. A comparison of Abs at 276 nm across doses is shown in Fig. 1c. Abs at 276 nm increases sharply when going from 0 to 30 kGy (for all three technologies) but increases only mildly from 30 to 60 kGy (as can be observed for Gamma and E-beam irradiated samples) or even decreases (in the case of X-ray irradiated samples). The changes in the shape of UV curve and the increases in Abs values below 290 nm are related to decomposition of antioxidants in the multilayer film[21]. Many such additives degrade upon irradiation into byproducts[22,23] that contribute to UV spectral changes.

As shown in Fig. 1b, c, the radiation sources resulted in varying amounts of increase in Abs below 290 nm. Abs of gamma-irradiated films were highest while those of e-beam were lowest. It should be noted that the observed increase in Abs below 290 nm will not necessarily cause malperformance of the irradiated product, especially when the irradiation doses are lower than 100 kGy which are far below the dose required to cause photodegradation of bulk polymers[24,25]. Assuming that the observed increase in Abs is attributed to degradation of the additives, the fact that the Abs below 290 nm increased fastest after gamma irradiation indicates that the alternative technologies (e-beam and X-ray) caused less degradation of antioxidants than the conventional accepted technology (gamma) at the same dose.

Melting and relaxation temperatures

Thermal properties of EVA and EVOH components in the multilayer films were studied in temperature scans by differential scanning calorimetry (DSC) and dynamic mechanical analysis (DMA) with tensile fixture. Representative signals are plotted in Fig. 2 for an unirradiated film. Other DSC and DMA curves of irradiated films and dose dependencies of thermal properties are given in the Supplementary Fig. 1.

Features in DSC and DMA plots can reflect certain molecular events. The characteristic signals in the same temperature range are compared and interpretated in Table 2. EVA exhibits rich thermal behaviors including melting and second-order relaxations. The γ transition typically occurs in the temperature range of −150 °C to −100 °C in polyethylene (PE) and ethylene copolymers[26–28]. Schatzki[29] proposed the famous "crankshaft" motion involving four methylene groups as the molecular mechanism for γ transition. The β transition observed between −40 °C and 10 °C is also characteristic of semi-crystalline ethylene copolymers and polyethylene containing structural irregularities such as branching[27,28,30,31]. Popli[30] and Mandelkern[32] attributed the β transition

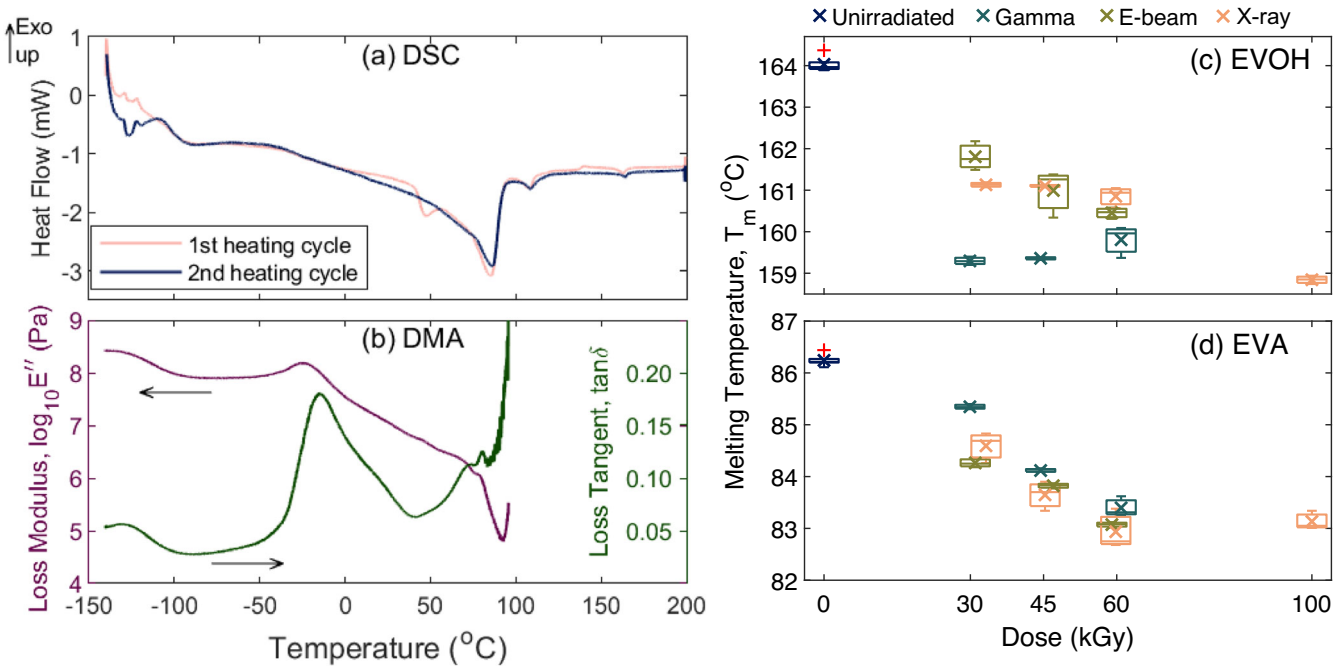

Fig. 2 Thermal properties of EVA/EVOH/EVA films. a Heat flow during two heating cycles measured on DSC and **b** loss modulus (E'') and tangent delta (tanδ) signals measured on DMA for an unirradiated EVA/EVOH/EVA film. Melting temperatures (T_m) of **c** EVOH and **d** EVA determined from DSC endothermic peaks. On each box, the cross indicates the sample mean, the central line is the median, the bottom and top bounds of the box represent the 25th and 75th percentiles, the whiskers extend to the extreme values which are within 1.5 times the interquartile range away from the box bounds, and the red plus sign indicates outlier that is a value more than 1.5 times the interquartile range away from the bounds of the box.

to the segmental relaxation of molecules at the interfacial regions associated with the crystallites. Although the molecular origin of the β transition is different from that of glass transition, β transition temperatures (T_β) of EVA have often been reported as glass transition temperature (T_g) in literature[33–35]. None of these second-order relaxation temperatures showed dependences on dose or irradiation technologies, as can be seen from Supplementary Figs. 2–4.

It has been reported that T_m and degree of crystallinity (χ_c) of EVA are affected by environmental aging[16,36,37]. In this study, we observed a decrease in T_m (Fig. 2d) and no change in χ_c (Supplementary Fig. 5a) with irradiation dose. Specifically, T_m of EVA decreased from that of the non-irradiated material by 1–2 °C with the first irradiation dose (30 kGy), by 3 °C up to 60 kGy, and did not further decrease when X-ray dose increased to 100 kGy, as shown in Fig. 2d. Reduction in T_m during irradiation is often explained by radiation-induced crosslinking in the polymer amorphous phase that restricts rearrangement of EVA chains and hinders growth of crystallites[38–41]. However, crosslinking in the amorphous phase would cause an increase of T_g[39,42] and a reduction in heat of fusion (ΔH_m) or χ_c, neither of which was observed to change with absorbed dose in this study as shown in Supplementary Figs. 3 and 5. To figure out the possible mechanism causing a decrease in T_m without changing T_g or χ_c, extensive literature studies were performed on semi-crystalline polymers especially PE and ethylene copolymers possessing molecular structures similar to that of EVA. Zoepfl et al. reported a 7 °C decrease in the T_m of high-density polyethylene (HDPE) after 1-MGy irradiation, where crosslinking only induced a decrease in T_m of less than 1 °C[43]. It was proposed that the additional 6 °C decrease in T_m of HDPE was related to the decrease in mean lamellar thickness and the broadening of lamellar thickness distribution on recrystallization[43]. Assuming that the shape of a melting endothermic peak in a DSC trace reflects the lamellar thickness distribution, and that the peak location is associated with the melting of the lamellar of the largest population[37,43], it is likely that the decrease in T_m of EVA observed in Fig. 2d was caused by a decrease in mean lamellar thickness. In that case, the effect of irradiation on the melting behavior of EVA is not remarkable, since the decrease in T_m (3 °C) was much smaller than the span of the endothermic peak (~50 °C).

Melting of EVOH manifested in the DSC curves as a small peak around 165 °C since the EVOH layer constitutes only 1.4% of the thickness of the multi-layer film. The T_m of EVOH decreased after irradiation but followed different trends for different source technologies as shown in Fig. 2c. The T_m of EVOH following gamma irradiation decreased the most with dose, which dropped by 4~5 °C after exposure to doses of 30~60 kGy. The T_m of e-beam and X-ray irradiated EVOH films decreased by 2~3 °C at intermediate doses (30~60 kGy). The decreasing trend of e-beam data appeared more progressive and more linearly correlated with dose than the others. The machine sources (e-beam and X-ray) posed smaller effects on T_m of EVOH than gamma rays at the same dose levels. The X-ray irradiated films exhibited a 5 °C drop in T_m of EVOH at 100 kGy, equivalent to 30 kGy gamma irradiation.

Stress-strain response in uniaxial extension

The stress-strain behavior of EVA/EVOH/EVA films exhibited anisotropy in tension. Such anisotropic response was related to semi-crystalline structure of the ethylene copolymer, and was also observed in a previous study on the same materials[44]. As shown in Fig. 3, specimens tested in the film machine direction (MD) exhibited higher stiffness and earlier breakage than specimens tested in the transverse direction (TD). The anisotropy is typical for blow extruded semi-crystalline polymers[44,45]. In the blowing process, chain orientation can occur in the melt state under shear stress, but can also relax before cooling to the crystallization temperature[45]. For the particular specimens studied in this work, no preferred orientation of crystals was observed prior to tensile

Table 2. Interpretations of characteristic signals on DSC and DMA temperature scan responses.

Temperature Range (°C)	DSC signal	DMA signal	Molecular origins
−130 to −100	Slope change in baseline ($\Delta C_p > 0.5\ J^{-1}g^{-1}\ °C$)	*E*″ and tanδ peak (truncated)	γ transition (relaxation of methylene groups)[28,31,62,63]
−40 to 0	Slope change	Broad *E*″ and tanδ peaks	β transition, glass transition (segmental relaxation within interfacial region)[28,30–32,64]
Near 15	-	Tanδ shoulder	Relaxation of rigid amorphous fraction[63,65]
40 to 50	Endothermic peak in the first heating cycle	-	Melting of imperfect EVA crystals[62]
Near 90	Broad endothermic peak	Onset of softening	EVA melting
Near 110	Small endothermic peak	-	PE melting*
Near 165	Small endothermic peak	-	EVOH melting

*PE is used as a tie layer between EVA and EVOH layers in the multilayer film studied.

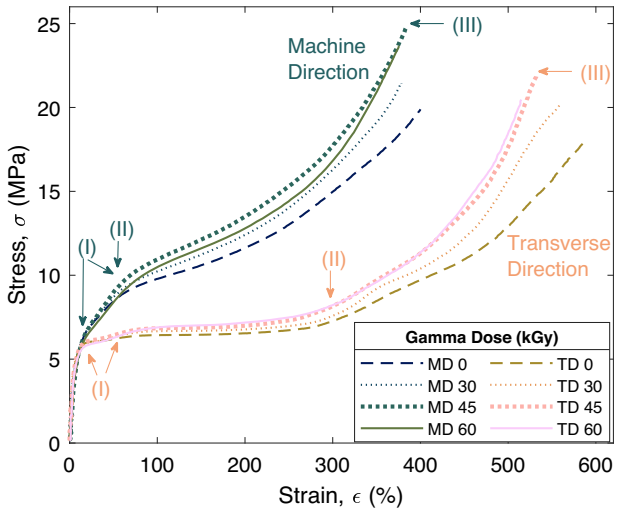

Fig. 3 Stress-strain responses of gamma-irradiated EVA/EVOH/EVA films under uniaxial tensile loading at a nominal strain rate of 1000% min^{-1}. All curves featured (I) yielding, (II) onset of strain hardening, and (III) ultimate breakage. The films were drawn in the machine direction (MD) and in the transverse direction (TD). One curve out of five repeats was plotted at each dose.

tests from SEM images[44], indicating that chains were fully relaxed to an isotropic state before folding themselves into lamellae.

Four characteristic regions could be found in the tensile responses as shown in Fig. 3, including an elastic deformation region before point (I), double yielding points at (I), a plateau region between (I) and (II), and a strain hardening region between (II) and (III). TD and MD specimens in their respective elastic and strain hardening regions exhibited similar behaviors. Double yielding labeled by points (I), instead of a sharp or well-defined yield point, was observed for both MD and TD specimens. The double yielding or a diffused yield region has been reported for polyethylene[46–48] and ethylene copolymers[44,49,50]. Bifurcation in stress-strain curves of MD and TD specimens was most apparent in the yield and post-yield regions, between point (I) and (II) in Fig. 3. A plateau existed for TD specimens ranging from below 100% to 300% strain where the stress was approximately constant at 6 MPa, but such a plateau was absent for MD specimens. Two mechanisms are found in literature to explain the plastic deformation of semi-crystal polymers in yield and post-yield regions. The first involves crystal block shearing, slipping, and lamellar fragmentation[47,51,52]. The second mechanism considers semi-crystalline polymers as a network with amorphous chains confined in a lamellae skeleton, where partial melting and recrystallization could be induced by stress in the post-yield region[48,53]. Despite the debate in mechanisms, the absence of a plateau region in MD specimens indicates that a certain degree of plastic deformation had occurred before tensile testing so that the material directly entered the strain-hardening region after yield. A possible pre-test deformation history of MD specimens could include drawing and rolling at a temperature below T_m.

From the stress-strain curves, mechanical properties including ultimate tensile strength (UTS), tensile elongation at break (EAB), secant modulus ($Es_{100\%}$), and tensile toughness (U_T) were calculated for TD and MD specimens separately, and compared to evaluate the material compatibilities of radiation technologies in Supplementary Figs. 6–9. UTS and $Es_{100\%}$ of irradiated samples were higher than those of unirradiated samples, but the increasing trend was not monotonic with respect to dose. EAB was observed to decrease with dose and the amounts of decrease was larger for TD samples. The phenomena were consistent with the assumed mechanism for the decrease in T_m, i.e., a decrease in mean lamellar thickness upon recrystallization, which would allow the molecular chains more closely packed and to contribute to macroscopic stiffness. Likewise, and according to TOST results listed in Table 1, equivalence can be claimed for effects of gamma vs. e-beam and X-ray irradiations on UTS and EAB, while the changes in $Es_{100\%}$ and U_T induced by gamma vs. e-beam and X-ray were not different based on *t*-test results.

Other material properties

In addition to the UV absorbance, thermal, and mechanical responses discussed above, material properties and indicators sensitive to polymer structure modification were also investigated, such as yellowness index, total color difference, carbonyl index, and surface free energy. Results are shown in the Supplementary Figs. 10–12. These properties did not change significantly with irradiation up to 60 kGy. There was also no difference between gamma and e-beam or X-ray irradiation on these properties.

DISCUSSION

Material compatibilities of the EVA/EVOH/EVA multilayer films with gamma, e-beam, and X-ray irradiations were examined via tensile tests, thermal analysis, UV-Vis and FTIR spectroscopy, discoloration, and surface energy. Signature thermal behaviors of a semi-crystalline ethylene copolymer were observed from temperature scans on DSC and DMA, including β and γ relaxations and melting. Stress-strain curves obtained from uniaxial tensile testing exhibited anisotropic responses, where a plateau ranging from 100% to 300% strain in between yielding and post-yield hardening regions was observed for TD samples but not for MD samples. The anisotropy in tensile responses was associated with blown

extrusion process. While most material properties did not change with dose, UV absorbance (Abs) in short wavelengths ($\lambda < 290$ nm), T_m of EVA and T_m of EVOH were found most sensitive to irradiation. Mechanical properties especially EAB were slightly altered by irradiation. The changes in thermal and mechanical properties were attributed to a decrease in mean lamellar thickness by radiation, while Abs increased as by-products accumulated from degradation of antioxidant additives. No photochemical degradation of the polymer matrix was observed up to 60 kGy of irradiation.

According to TOST results where industrial equivalence criteria were available, all five material properties were equivalently affected by the accelerator-based radiation technologies (e-beam and X-ray) and the more commonly used radioisotope technology (gamma), as listed in Table 1. Equivalency criteria were defined only on independent results (e.g. no criteria for toughness which combines both UTS and EAB behaviors). No equivalency criteria can be defined for spectroscopic data as well. It means that 5 out of 12 measurements can be treated independently with TOST. A parallel conclusion regarding material compatibility was investigated based on the classic t-test results, and the current conclusion is that the changes in all investigated material properties, except T_m and Abs, caused by e-beam and X-ray and the changes caused by gamma irradiation were not different. Abs in short wavelengths ($\lambda < 290$ nm) and melting behaviors were examined more closely as *t*-tests did not determine with current datasets if effects of the technologies on these two properties were equivalent (see Table 1). However, as described in Results section, changes in short-wavelength Abs and in T_m of EVOH caused by e-beam and X-ray were milder than those caused by gamma at the same dose, which indicates that e-beam and X-ray would induce less modifications of the investigated multilayer films, and supports viability of e-beam and X-ray as alternative options to gamma for radiation sterilization. Changes in T_m of EVA induced by irradiation (<3 °C) were most probably caused by a decrease in mean lamellar thickness, and were insignificant compared to the broadness of the melting peak (50 °C from onset to endset). In summary, there is no barrier to replacing cobalt gamma with alternative technologies of e-beam or X-ray for sterilizing the EVA/EVOH/EVA films based on the material compatibilities investigated in this study.

When the objective of a statistical hypothesis test is to conclude that groups are equivalent, an equivalence test should be utilized, such as the two one-sided *t*-test (TOST)[54]. An equivalence test forces identification from a practical perspective of how large of a difference is significant and puts the burden on the data to reach a conclusion of equivalence. The design of an equivalence test can be challenging because the analyst must define an acceptance criterion on the basis of prior knowledge of the measurement as well as its intended application[55]. In addition to the acceptance criteria proposed in Table 1 and by Tavlet et al.[56], there remains a need for criteria, industrial standards, and quantified acceptance limits in terms of material properties to guide the procedure of using alternative technologies for sterilization or for other comparison purposes. The CERN[56] proposed initial categorization of radiation resistance with a criterion of 50% loss in elongation at break (EAB). The Association for the Advancement of Medical Instrumentation (AAMI) technical information report (TIR 17)[24] is another source of guidance, wherein the criterion for material compatibility considers 25% EAB reduction[24]. Criteria in terms of other common material properties sensitive to polymer degradation such as yellowing and carbonyl index change were not found.

To further dive into mechanistic insights, relations between the molecular structure and measured material properties should be verified. For example, directly measuring crystal orientation and lamellar thickness by imaging techniques could help reveal the changes in crystal morphology induced by irradiation.

METHODS

Material

The samples are multilayer films composed of ethylene vinyl acetate (EVA) layers sandwiching an ethylene vinyl alcohol (EVOH) layer, commercially known as S71 film provided by Sartorius Stedim FMT S.A.S. Figure 4 shows the sandwich structure and thickness of each layer, being 320 µm/5 µm/35 µm for EVA/EVOH/EVA. Polyethylene (PE) is used as tie layer between EVA and EVOH layers. The EVOH layer contains 56 mol% vinyl alcohol. The direction along which the film was blow extruded is denoted as the "machine direction" (MD), whereas the "transverse direction" (TD) is perpendicular to machine direction.

Radiation processing

EVA/EVOH/EVA samples were pre-cut before irradiated in gamma, e-beam, and X-ray facilities. Before irradiation, samples were packed and wrapped in 100 ± 20 µm thick packaging bags made of polyethylene (PE)/polyamide (PA)/PE so that a partial vacuum, though not controlled, was formed. Packaging bags were not degassed and therefore contained some level of oxygen around samples. The bags were thermo-sealed, placed in a cardboard box, and then irradiated. After irradiation and before material testing, the cardboard box was stored in the dark room. The temperature of the dark room was controlled at 23 ± 2 °C. The doses delivered to sample surfaces are given in Table 3.

Gamma irradiation was carried out at room temperature (approximately 40 °C) with a cobalt-60 source at Ionisos (Dagneux, France) with an average dose rate of 1–2 kGy/h. Multiple sterilization cycles were performed to obtain target doses, the waiting time between which as well as the storage condition were not controlled. The actual delivered dose (absorbed dose to water) was measured using calibrated alanine dosimeters on a cardboard box simulating the irradiation geometry of the samples. The uncertainty in the provided dose values for samples is approximately ±5% at the 95% confidence level. Standard practice ISO/ASTM 51702 was followed as applicable[57].

The e-beam irradiation was performed using two 10 MeV, 20 kW Mevex accelerators at Steri-Tek (Fremont, California, USA). The sample packaging was oriented perpendicular relative to the

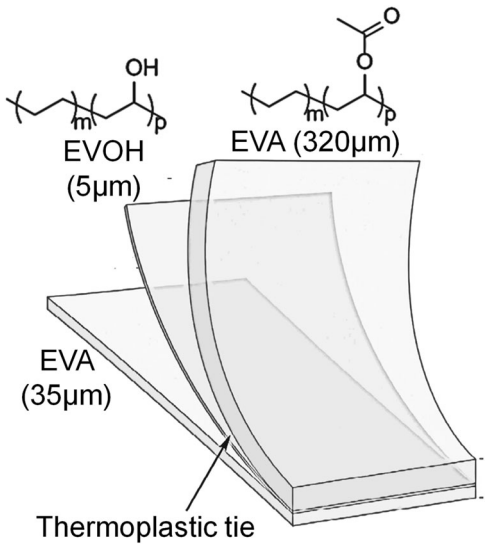

Fig. 4 Structure of EVA/EVOH/EVA multilayer film sample. The samples used in this study are multilayer films composed of ethylene vinyl acetate (EVA) layers sandwiching the ethylene vinyl alcohol (EVOH) layer. The thickness of each layer is 320 µm/5 µm/35 µm. Polyethylene (PE) is used as the thermoplastic tie layer between EVA and EVOH.

Table 3. Doses delivered to surface of films. "N/A": not available.

Target Dose (kGy)	Gamma (kGy)	E-beam (kGy)	X-ray (kGy)
30	29.9 ± 1.3	31.0 ± 1.6	33.2 ± 0.4
45	44.4 ± 0.2	47.0 ± 2.4	45.3 ± 0.6
60	60.9 ± 0.8	59.0 ± 3.0	59.8 ± 1.1
100	N/A	N/A	98.9 ± 0.7

incident radiation beam[58], and the average dose rate is estimated to be approximately 3 kGy s^{-1}. The ambient temperature during irradiation is estimated to be approximately 25 °C. Calibrated model B3 dosimeters were used on cardboard boxes simulating the irradiation geometry to assess the radiation delivered to the film samples (absorbed dose to water). Standard practice ISO/ASTM 51649 was followed as applicable[59].

X-ray irradiation was performed with a 7 MeV Rhodotron accelerator at Aerial (Strasbourg, France) with an average dose rate of 15 kGy h^{-1} using double-sided irradiation, and an estimated ambient temperature of approximately 35 °C. Alanine dosimeters (calibrated in terms of absorbed dose to water) were placed on the actual samples. Standard practice ISO/ASTM 51608 was followed as applicable[60].

Tensile test

Tensile tests were performed following ASTM D882 and ISO 527 standards. Force was measured on an Instron Model 4943 universal test machine equipped with 1 kN load cell and pneumatic grips. Each specimen was 100 mm × 25 mm × 0.36 mm. Serrated grips were mounted 25 mm from each end. The initial distance between grips was 50 mm. A small preload of 1.5 N was applied with a pull rate of 3 mm min^{-1}. Strain was calculated from the video recorded on a Canon EOS Rebel T7i digital camera. Four dark lines across the width were painted on the specimens for pixel strain calculation. To enhance video extensometry results, a white background was placed behind the specimen. The nominal pull rate was 5 mm min^{-1} for the first 2% and 500 mm min^{-1} for the remaining of the experiment until the specimen broke. Elongation at break (EAB), ultimate tensile stress (UTS), and toughness (U_T) were determined from the last point before breaking. Secant modulus at 100% strain ($Es_{100\%}$), instead of Young's modulus, was reported due to lack of Hookean region on the stress-strain curve. The yield point conventionally defined as $\delta\sigma/\delta\varepsilon = 0$ or by an offset yield method was not applicable.

Differential scanning calorimetry (DSC)

Thermal properties were measured using a Differential Scanning Calorimeter (DSC, TA Instruments Q2000). Approximately 5 mg of specimen was sealed in a Tzero pan. Between −140 °C and 200 °C, a cyclic heating-cooling-reheating protocol was used to ensure consistent thermal history. The heating and cooling rates were 10 °C min^{-1}. Thermal properties were extracted from the second heating ramp. Relaxation temperatures, including the glass transition temperature (T_g), were determined as the midpoint of a step change in heat flow. Melting temperatures (T_m) were determined from endothermic peaks. Degree of crystallinities (χ_c) of EVA and EVOH were calculated as the ratio of heat of fusion (ΔH_f) measured on endothermic peaks to heat of fusion of 100% crystalized PE and polyvinyl alcohol (PVOH) (ΔH_f^0), being 290 J g^{-1} [61] and 156.2 J g^{-1} [61] respectively. The ΔH_f^0 of PE was used to calculate χ_c of EVA since only ethylene segments in EVA can crystallize and polyvinyl acetate (PVA) does not crystallize. Ratio of heat of fusion was normalized by thickness (t) of each layer, which was proportional to mass assuming density of EVA and EVOH layers were the same.

Dynamic mechanical analysis (DMA)

Dynamic mechanical analysis (DMA, TA Instruments Q800) was used to determine relaxation temperatures such as T_g. Temperature readings of DMA were calibrated with a thermometer at 22.8 °C and by the melt of Indium at 156.6 °C. Specimens pre-cut into 30 mm × 6 mm × 0.36 mm were mounted in a tension geometry. The distance between clamps was approximately 15 mm. A temperature scan from −140 °C to 110 °C at 2 °C min^{-1} was performed, with an oscillation amplitude of 0.1% strain and a frequency of 1 Hz. An underlying force was used to keep the specimen taut, being 10 N at the lowest temperature and decreasing at higher temperatures as proportional to measured stiffness. β and γ transition temperatures were determined from tanδ peaks.

UV-Vis spectrometry

UV-Vis transmittance (T) at 200–800 nm was measured on an Agilent Cary 5000 UV-Vis-NIR spectrophotometer with solid sample accessory. Absorbance (A) was calculated based on Eq. (1).

$$A = \log_{10}\frac{1}{T} \tag{1}$$

Tristimulus colors in terms of CIE 1931 XYZ were calculated from visible spectrum (380–780 nm) following Eqs. (2)–(5) with parameters at 5 nm interval provided in ASTM E308. CIE 1967 L*a*b* color space is converted from XYZ values in MATLAB *xyz2lab* function. Single-value matrices, including yellowness index (YI) and total color difference (ΔE^*_{ab}), were obtained based on Eqs. (6) and (7).

$$X = k\sum_{\lambda} R(\lambda)S(\lambda)\bar{x}(\lambda)\Delta\lambda \tag{2}$$

$$Y = k\sum_{\lambda} R(\lambda)S(\lambda)\bar{y}(\lambda)\Delta\lambda \tag{3}$$

$$Z = k\sum_{\lambda} R(\lambda)S(\lambda)\bar{z}(\lambda)\Delta\lambda \tag{4}$$

$$k = 100/\sum_{\lambda} S(\lambda)\bar{y}(\lambda)\Delta\lambda \tag{5}$$

$$YI = \frac{100(C_X X - C_Z Z)}{Y}\begin{cases} C_X = 1.2985 \\ C_Z = 1.1335 \end{cases}(D65, 1931) \tag{6}$$

$$\Delta E^*_{ab} = \sqrt{\left(L^* - L^*_{ref}\right)^2 + \left(a^* - a^*_{ref}\right)^2 + \left(b^* - b^*_{ref}\right)^2} \tag{7}$$

Fourier transform infrared spectrometry (FTIR)

Absorbance at 4000–500 cm^{-1} was measured on a Fourier Transform Infrared (FTIR) Spectrometer (Bruker Alpha II) with an attenuated total reflection (ATR) accessory. Four locations on each specimen were tested with 64 scans at a resolution of 4 cm^{-1}. Carbonyl index (CI) was calculated based on Eq. (8) as a ratio of absorbance of carbonyl groups ($A_{C=O}$) and hydroxyl groups ($A_{C\text{-}H}$), peak values of which were found in the range of 1650–1830 cm^{-1} and 1400–1510 cm^{-1} respectively.

$$CI = \frac{A_{C=O}}{A_{C-H}} \tag{8}$$

Surface free energy

Surface energy measurements were performed using a Krüss Mobile Surface Analyzer (MSA) equipped with ADVANCE software and diiodomethane (Thermo Scientific; >99% purity) and distilled

water syringes. Measurements were performed in quintuplicate using the double sessile drop program and an unmodified version of the automation program provided with the ADVANCE software. Droplet size (2 µL target) was calibrated every 10 measurements. Contact angles were measured using the automatic baseline function and the ellipse (tangent^{-1}) fitting method. Erroneous contact angle measurements were corrected by the manual baseline method. Surface free energy was calculated using the Owens, Wendt, Rabel, and Kaelbe (OWRK) method with a correlation coefficient of 1.00. Additional parameter accounting for microscale surface roughness was not used in this work.

DATA AVAILABILITY

All data generated or analyzed during this study are included in this published article and its Supplementary Information files.

CODE AVAILABILITY

The codes used in this study for statistical analysis and data visualization can be made available upon request from the corresponding author.

Received: 30 May 2023; Accepted: 9 November 2023;
Published online: 01 December 2023

REFERENCES

1. Gamma Industry Processing Alliance, (GIPA) & International Irradiation Association, (iia). A Comparison of Gamma, E-beam, X-ray and Ethylene Oxide Technologies for the Industrial Sterilization of Medical Devices and Healthcare Products. https://gipalliance.net/wp-content/uploads/2013/01/GIPA-WP-GIPA-iia-Sterilization-Modalities-FINAL-Version-2017-October-308772.pdf (2017).
2. Lieberman, J. et al. Replacement of cobalt in medical device sterilization: current trends, opportunities and barriers to adoption of X-ray and E-beam within the medical device sterilization market. *Arab. J. Nucl. Sci. Appl.* **53**, 102–111 (2020).
3. Kroc, T. K., Thangaraj, J. C. T., Penning, R. T. & Kephart, R. D. Accelerator-driven medical sterilization to replace Co-60 sources. https://lss.fnal.gov/archive/2017/pub/fermilab-pub-17-314-di.pdf (2017).
4. Tallentire, A. & Miller, A. Microbicidal effectiveness of X-rays used for sterilization purposes. *Radiat. Phys. Chem.* **107**, 128–130 (2015).
5. McEvoy, B. et al. Studies on the comparative effectiveness of X-rays, gamma rays and electron beams to inactivate microorganisms at different dose rates in industrial sterilization of medical devices. *Radiat. Phys. Chem.* **208**, 110915 (2023).
6. Fifield, L. S. et al. Direct comparison of gamma, electron beam and X-ray irradiation effects on single-use blood collection devices with plastic components. *Radiat. Phys. Chem.* **180**, 109282 (2021).
7. Menzel, R., Dorey, S., Maier, T., Pahl, I. & Hauk, A. X-ray sterilization of biopharmaceutical manufacturing equipment—Extractables profile of a film material and copolyester Tritan™ compared to gamma irradiation. *Biotechnol. Prog.* https://doi.org/10.1002/btpr.3214 (2021).
8. Rabek, J. F. Polymer photodegradation: mechanisms and experimental methods. (Springer Dordrecht, 2012).
9. Vohlídal, J. Polymer degradation: a short review. *Chem. Teach. Int.* **3**, 213–220 (2021).
10. Yousif, E. & Haddad, R. Photodegradation and photostabilization of polymers, especially polystyrene: review. *Springerplus* **2**, 1–32 (2013).
11. Allen, N. S., Edge, M. & Hussain, S. Perspectives on yellowing in the degradation of polymer materials: inter-relationship of structure, mechanisms and modes of stabilisation. *Polym. Degrad. Stab.* **201**, 109977 (2022).
12. Gaston, F., Dupuy, N., Girard-Perier, N., Marque, S. R. A. & Dorey, S. Investigations at the product, macromolecular, and molecular level of the physical and chemical properties of a γ-irradiated multilayer EVA/EVOH/EVA film: comprehensive analysis and mechanistic insights. *Polym. (Basel)* **13**, 2671 (2021).
13. Gaston, F., Dupuy, N., Marque, S. R. A., Barbaroux, M. & Dorey, S. FTIR study of ageing of γ-irradiated biopharmaceutical EVA based film. *Polym. Degrad. Stab.* **129**, 19–25 (2016).
14. Czanderna, A. W. & Pern, F. J. Encapsulation of PV modules using ethylene vinyl acetate copolymer as a pottant: a critical review. *Sol. Energy Mater. Sol. Cells* **43**, 101–181 (1996).
15. Allen, N., Edge, M., Rodriguez, M., Liauw, C. M. & Fontan, E. Aspects of the thermal oxidation, yellowing and stabilisation of ethylene vinyl acetate copolymer. *Polym. Degrad. Stab.* **71**, 1–14 (2000).
16. Jin, J., Chen, S. & Zhang, J. UV aging behaviour of ethylene-vinyl acetate copolymers (EVA) with different vinyl acetate contents. *Polym. Degrad. Stab.* **95**, 725–732 (2010).
17. Barretta, C., Oreski, G., Feldbacher, S., Resch-Fauster, K. & Pantani, R. Comparison of degradation behavior of newly developed encapsulation materials for photovoltaic applications under different artificial ageing tests. *Polym. (Basel)* **13**, 271 (2021).
18. Landete-Ruiz, M. D. & Martín-Martínez, J. M. Surface modification of EVA copolymer by UV treatment. *Int. J. Adhes. Adhes.* **25**, 139–145 (2005).
19. Meyners, M. Equivalence tests–a review. *Food Qual. Prefer.* **26**, 231–245 (2012).
20. Jiang, S., Wang, K., Zhang, H., Ding, Y. & Yu, Q. Encapsulation of PV modules using ethylene vinyl acetate copolymer as the encapsulant. *Macromol. React. Eng.* **9**, 522–529 (2015).
21. Audran, G., Dorey, S., Dupuy, N., Gaston, F. & Marque, S. R. A. Degradation of γ-irradiated polyethylene-ethylene vinyl alcohol-polyethylene multilayer films: an ESR study. *Polym. Degrad. Stab.* **122**, 169–179 (2015).
22. Gaston, F., Dupuy, N., Marque, S. R. A., Gigmes, D. & Dorey, S. Monitoring of the discoloration on γ-irradiated PE and EVA films to evaluate antioxidant stability. *J. Appl. Polym. Sci.* **135**, 46114 (2018).
23. Tao, B. et al. Determination of the contents of antioxidants and their degradation products in sodium chloride injection for blood transfusion. *J. Anal. Methods Chem.* **2020**, 8869576 (2020).
24. Association for the Advancement of Medical Instrumentation (AAMI). Compatibility of materials subject to sterilization (AAMI TIR17:2017). https://doi.org/10.2345/9781570207006.ch1 (2017).
25. Clough, R. L., Gillen, K. T. & Dole, M. *Radiation resistance of polymers and composites*. (Elsevier Applied Science, 1991).
26. McKenna, L. W., Kajiyama, T. & MacKnight, W. J. The γ relaxation of a poly (ethylene-co-methacrylic acid) polymer and its salts. *Macromolecules* **2**, 58–61 (1969).
27. Boyd, R. H. Relaxation processes in crystalline polymers: experimental behaviour — a review. *Polym. (Guildf.)* **26**, 323–347 (1985).
28. Khonakdar, H. A., Wagenknecht, U., Jafari, S. H., Hässler, R. & Eslami, H. Dynamic mechanical properties and morphology of polyethylene/ethylene vinyl acetate copolymer blends. *Adv. Polym. Technol.* **23**, 307–315 (2004).
29. Schatzki, T. F. Statistical computation of distribution functions of dimensions of macromolecules. *J. Polym. Sci.* **57**, 337–356 (1962).
30. Popli, R. & Mandelkern, L. The transition in ethylene copolymers: the β-transition. *Polym. Bull.* **9**, 260–267 (1983).
31. Brogly, M., Nardin, M. & Schultz, J. Effect of vinylacetate content on crystallinity and second-order transitions in ethylene—vinylacetate copolymers. *J. Appl. Polym. Sci.* **64**, 1903–1912 (1997).
32. Mandelkern, L. The relation between structure and properties of crystalline polymers. *Polym. J.* **17**, 337–350 (1985).
33. Agroui, K., Collins, G. & Farenc, J. Measurement of glass transition temperature of crosslinked EVA encapsulant by thermal analysis for photovoltaic application. *Renew Energy* **43**, 218–223 (2012).
34. Puente, J. A. S. et al. Segmental mobility and glass transition of poly(ethylene-vinyl acetate) copolymers: Is there a continuum in the dynamic glass transitions from PVAc to PE? *Polym. (Guildf.)* **76**, 213–219 (2015).
35. Arsac, A., Carrot, C. & Guillet, J. Rheological characterization of ethylene vinyl acetate copolymers. *J. Appl. Polym. Sci.* **74**, 2625–2630 (1999).
36. Mihaylova, M. D., Nedkov, T. E., Krestev, V. P. & Kresteva, M. N. Supermolecular structure of poly(propylene-co-ethylene)/poly(ethylene-co-vinyl acetate) blends irradiated with fast electrons. SEM, SAXS and DSC studies. *Eur. Polym. J.* **37**, 2177–2186 (2001).
37. Shi, X.-M., Zhang, J., Li, D.-R. & Chen, S.-J. Effect of damp-heat aging on the structures and properties of ethylene-vinyl acetate copolymers with different vinyl acetate contents. *J. Appl. Polym. Sci.* **112**, 2358–2365 (2009).
38. Kusy, R. P. & Turner, D. T. Radiation Chemistry of polymers studied by depression of melting temperature. *Macromolecules* **4**, 337–341 (1971).
39. Zurina, M., Ismail, H. & Ratnam, C. T. Characterization of irradiation-induced crosslink of epoxidised natural rubber/ethylene vinyl acetate (ENR-50/EVA) blend. *Polym. Degrad. Stab.* **91**, 2723–2730 (2006).
40. Ramarad, S., Ratnam, C. T., Khalid, M., Chuah, A. L. & Hanson, S. Improved crystallinity and dynamic mechanical properties of reclaimed waste tire rubber/EVA blends under the influence of electron beam irradiation. *Radiat. Phys. Chem.* **130**, 362–370 (2017).
41. Matsui, T., Shimoda, M. & Osajima, Y. Mechanical changes of electron beam irradiated ethylene–vinyl acetate copolymer (EVA) film (I). *Polym. Int.* **29**, 85–90 (1992).

42. Zhang, X. C. & Cameron, R. E. The morphology of irradiated isotactic polypropylene. *J. Appl. Polym. Sci.* **74**, 2234–2242 (1999).
43. Zoepfl, F. J., Markovič, V. & Silverman, J. Differential scanning calorimetry studies of irradiated polyethylene: I. Melting temperatures and fusion endotherms. *J. Polym. Sci. Polym. Chem. Ed.* **22**, 2017–2032 (1984).
44. Dorey, S. et al. Effect of gamma irradiation on the oxygen barrier properties in ethyl-vinyl acetate/ethylene-vinyl alcohol/ethyl-vinyl acetate multilayer film. *J. Appl. Polym. Sci.* **137**, 49361 (2020).
45. Zhang, X. M., Elkoun, S., Ajji, A. & Huneault, M. A. Oriented structure and anisotropy properties of polymer blown films: HDPE, LLDPE and LDPE. *Polym. (Guildf.)* **45**, 217–229 (2004).
46. Popli, R. & Mandelkern, L. Influence of structural and morphological factors on the mechanical properties of the polyethylenes. *J. Polym. Sci. Part B Polym. Phys.* **25**, 441–483 (1987).
47. Seguela, R. & Rietsch, F. Double yield point in polyethylene under tensile loading. *J. Mater. Sci. Lett.* **9**, 46–47 (1990).
48. Lucas, J. C., Failla, M. D., Smith, F. L., Mandelkern, L. & Peacock, A. J. The double yield in the tensile deformation of the polyethylenes. *Polym. Eng. Sci.* **35**, 1117–1123 (1995).
49. Kennedy, M. A., Peacock, A. J., Failla, M. D., Lucas, J. C. & Mandelkern, L. Tensile properties of crystalline polymers: random copolymers of ethylene. *Macromolecules* **28**, 1407–1421 (1995).
50. Graham, J. T., Alamo, R. G. & Mandelkern, L. The effect of molecular weight and crystallite structure on yielding in ethylene copolymers. *J. Polym. Sci. Part B Polym. Phys.* **35**, 213–223 (1997).
51. Mercier, J. P., Zambelli, G. & Kurz, W. Chapter 12 - Factors influencing mechanical properties. In *Introduction to Materials Science* (eds. Mercier, J. P. Zambelli, G. & Kurz, W.) 279–320 (Elsevier, 2002).
52. Hiss, R., Hobeika, S., Lynn, C. & Strobl, G. Network stretching, slip processes, and fragmentation of crystallites during uniaxial drawing of polyethylene and related copolymers. A comparative study. *Macromolecules* **32**, 4390–4403 (1999).
53. Men, Y., Rieger, J. & Strobl, G. Role of the entangled amorphous network in tensile deformation of semicrystalline polymers. *Phys. Rev. Lett.* **91**, 95502 (2003).
54. Lakens, D. Equivalence tests: a practical primer for t tests, correlations, and meta-analyses. *Soc. Psychol. Personal. Sci.* **8**, 355–362 (2017).
55. Limentani, G. B., Ringo, M. C., Ye, F., Bergquist, M. L. & McSorley, E. O. Beyond the t-test: statistical equivalence testing. *Anal. Chem.* **77**, 221A–226A (2005).
56. Tavlet, M., Fontaine, A. & Schönbacher, H. Compilation of radiation damage test data. Index des résultats d'essais de radiorésistance; 2nd ed. https://doi.org/10.5170/CERN-1998-001 (1998).
57. ISO/ASTM 51702:2013. Practice for dosimetry in a gamma facility for radiation processing. https://www.iso.org/standard/61086.html (2013).
58. Dupuy, N. et al. Supplementing gamma sterilization with x-ray and e-beam technologies: an international industry and academia collaboration. *BioProcess International* **20** https://bioprocessintl.com/2022/march-2022/supplementing-gamma-sterilization-with-x-ray-and-e-beam-technologies-an-international-industry-and-academia-collaboration (2022).
59. ISO/ASTM 51649:2015. Practice for dosimetry in an electron beam facility for radiation processing at energies between 300 keV and 25 MeV. https://www.iso.org/standard/66728.html (2015).
60. ISO/ASTM 51608:2015. Practice for dosimetry in an X-ray (bremsstrahlung) facility for radiation processing at energies between 50 keV and 7.5 MeV. https://www.iso.org/standard/66727.html (2015).
61. Lagaron, J. M., Gimenez, E., Saura, J. J. & Gavara, R. Phase morphology, crystallinity and mechanical properties of binary blends of high barrier ethylene–vinyl alcohol copolymer and amorphous polyamide and a polyamide-containing ionomer. *Polym. (Guildf.)* **42**, 7381–7394 (2001).
62. Stark, W. & Jaunich, M. Investigation of ethylene/vinyl acetate copolymer (EVA) by thermal analysis DSC and DMA. *Polym. Test.* **30**, 236–242 (2011).
63. Zhang, X., Yang, H., Song, Y. & Zheng, Q. Influence of crosslinking on crystallization, rheological, and mechanical behaviors of high density polyethylene/ethylene-vinyl acetate copolymer blends. *Polym. Eng. Sci.* **54**, 2848–2858 (2014).
64. Yamaki, S. B., Prado, E. A. & Atvars, T. D. Z. Phase transitions and relaxation processes in ethylene-vinyl acetate copolymers probed by fluorescence spectroscopy. *Eur. Polym. J.* **38**, 1811–1826 (2002).
65. Sung, Y. T. et al. Effects of crystallinity and crosslinking on the thermal and rheological properties of ethylene vinyl acetate copolymer. *Polym. (Guildf.)* **46**, 11844–11848 (2005).

ACKNOWLEDGEMENTS

This work was funded by the U.S. Department of Energy National Nuclear Security Administration Office of Radiological Security. The Pacific Northwest National Laboratory is operated by Battelle for the U.S. Department of Energy under Contract DE-AC05-76RL01830. The funder played no role in study design, data collection, analysis and interpretation of data, or the writing of this manuscript. Sartorius Stedim FMT S.A.S. is gratefully acknowledged for providing the multilayer films studied in this work. Authors would like to extend their appreciation to Ionisos, Steri-Tek, and Aerial for the gamma, e-beam, and X-ray irradiation processing.

AUTHOR CONTRIBUTIONS

Y.N. performed DSC, DMA, UV-Vis, and FTIR measurements, analyzed data and wrote the initial draft of manuscript. T.T.B. prepared samples and developed a video extensometry tool for strain calculation. K.H. performed mechanical tests. D.L. analyzed FTIR data and discussed results. W.K.F. measured surface free energy. S.K.C. performed statistical analysis using R packages. L.N. coordinated e-beam irradiation on samples. M.P. designed the study and discussed results. N.D. designed the study and discussed results. S.M. designed the study and discussed results. M.K.M. designed the study and discussed results. S.D.P. designed the study and discussed results. S.D. designed the study, discussed results, performed statistical analysis in Minitab and was a major contributor in writing the manuscript. L.S.F. designed the study, discussed results, and was a major contributor in writing the manuscript. All authors read and approved the final manuscript.

COMPETING INTERESTS

The authors declare no competing interests.

ADDITIONAL INFORMATION

Supplementary information The online version contains supplementary material available at https://doi.org/10.1038/s41529-023-00413-x.

Correspondence and requests for materials should be addressed to Yelin Ni, Samuel Dorey or Leonard S. Fifield.